ESPM 228, Advanced Topics in Biometeorology and Micrometeorology

Lecture 4 Micromet Flux Measurements, Eddy Covariance, Application, Part 2

Instructor:
Dennis Baldocchi,
Professor of Biometeorology
Ecosystems Science Division
Department of Environmental Science, Policy and Management
345 Hilgard
Baldocchi@berkeley.edu
642-2874

February 10, 2014

Evaluating the Flux Covariance

The power spectrum (also called the variance or energy spectrum) quantifies the amount of variance (or energy) associated with particular frequency or wavelength scales. The power spectrum of a scalar or a wind velocity component is derived through a Fourier transformation of a temporal (or spatial) series of a given variable. The Fourier transform converts the time (or space) series into a frequency (or wavelength) domain by representing it as an infinite sum of sine and cosine terms. Integration of spectral energy densities across the whole range of significant frequencies (or wavelengths) yields the total variance of the velocity component or scalar quantity under scrutiny.

$$\overline{w'w'} = \int_0^\infty S_{ww}(\omega)d\omega$$

In a similar manner the real component of the cross-spectrum, the co-spectrum, quantifies the amount of 'flux' that is associated with a particular scale.

$$F = \overline{w'c'} = \int_0^\infty S_{wc}(\omega)d\omega$$

A distinct property of turbulence in the natural environment is a wide spectrum of motion scales (eddies) associated with the fluid flow. The largest scales of turbulence are produced by forces driving the mean fluid flow. Dynamically instable, these large eddies break down into progressively smaller and smaller scales, via an inertial cascade. This cascading breakdown of eddy size continues until the eddies are so small that energy is consumed by working against viscous forces that convert kinetic energy into heat. Hence, in application, the method must acquire both short and long scale contributions to the turbulent flux.

ESPM 228, Advanced Topics in Biometeorology and Micrometeorology

The dependence of the variance or flux covariance on a spectrum of eddies imposes several constraints on instrument design, measurement principles and sensor sampling. Reviews and critiques of the eddy covariance method have been produced by numerous investigators. The reader is referred to them for further details [*Aubinet et al.*, 2000; *D.D. Baldocchi*, 2003; *D. D. Baldocchi et al.*, 1988; *Businger*, 1986; *Foken and Wichura*, 1996; *Goulden et al.*, 1996; *Loescher et al.*, 2006; *Massman and Lee*, 2002; *McMillen*, 1988]. With regard to sensor sampling attention and care must be paid towards:

a. sampling duration;
b. sampling frequency;
c. averaging method.

With regard to instrumental placement, design and implementation, the accuracy of any flux measurement will be influenced by:

1) sensor size
2) separation of instruments
3) placement, in terms of height and position in the constant flux layer
4) mechanical filtering or distortion of turbulence, as when sampling through a tube or when a tower or anemometer head interferes with the wind.
5) Rotation of coordinates to compute fluxes orthogonal to mean streamlines.
6) Flow interference by towers and booms.

A filtering of covariance signals occurs for several reasons. High frequency contributions are attenuated because sensors have a finite response time, their transducer may have a significant sampling volume or integral scale length (relative to scales of turbulence) or the pumping of air through a tube will distort the structure of eddies.

Filtering can be imposed through data acquisition because data acquisition systems use a discrete sampling interval. As a result they possess a finite cut-off, denoted at the high frequency end of the spectrum as the Nyquist frequency.

In practice, a measured covariance is a function of the true cospectrum (Co_{wc}) and a spectral transfer function (H), that arises from the issues discussed above:

$$\overline{w'c'}_{measured} = \int_{0}^{\infty} H(\varpi) Co_{wc}(\varpi) d\omega$$
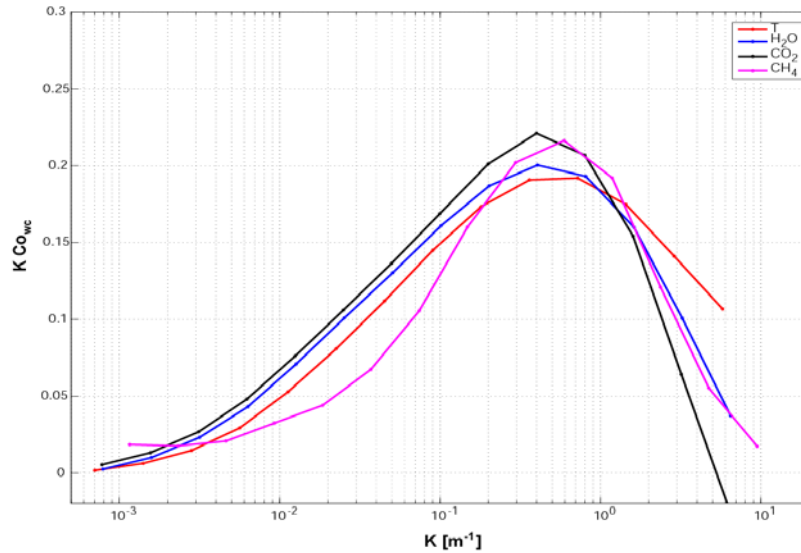
Figure 1 co-spectrum from study over peatland on Sherman Island. Co-spectra are shown for temperature, water vapor, CO2 and methane. Data of Detto and Baldocchi.

The transfer function H(w) is determined by the product of numerous filtering effects [*Massman*, 2000; *Moore*, 1986]:

$$H(\varpi) = H_1(\varpi)H_2(\varpi)...H_n(\varpi) = \prod_{n=1}^{N} H_n(\varpi)$$

The most important transfer functions that are applied to eddy covariance measurements include:

1. high pass filtering
2. low pass filtering
3. digital sampling at a limited frequency
4. sensor response time
5. fluctuation attenuation by sampling through a tube
6. Line or volume sampling
7. sensor separation

When computing filter and transfer functions one must be careful and not to confuse terminology. Moore [*Moore*, 1986] reports filtering gain functions (G) and transfer functions (T). When applied to correct a power spectrum the gain filters are squared.

Time Averaging, Detrending and High Pass Filtering

Since fluctuations from the mean are computed as the difference between instantaneous and mean values, we must assess the time series mean. This is not a trivial exercise due

to the multiple time scales associated with a time series. The basic rules of Reynolds averaging use arithmetic means. The application of Reynold's decomposition upon a time series, using a finite mean, imposes a band pass filter on the data [*Kaimal and Finnigan*, 1994]. Arithmetic means or digital recursive filters pass high frequency fluctuations but attenuate low frequency components in their attempt to assess means for mean removal calculations. Moore [*Moore*, 1986], Horst [*Horst*, 1997] and Massman [*Massman*, 2000] have developed schemes for estimating the amount of flux density lost by these 'filtering' effects.

Since concentrations and velocities experience a diurnal pattern, they are never at steady state. Some investigators, therefore, prefer to detrend a time series and using a trend line to remove the mean. The rules of Reynolds averaging, however, say nothing about detrending (K.T. Paw U, personal communication). They are based on arithmetic means. In my opinion, if there is a trend we should treat this with a modification of the Conservation Budget and account for it as a storage term.
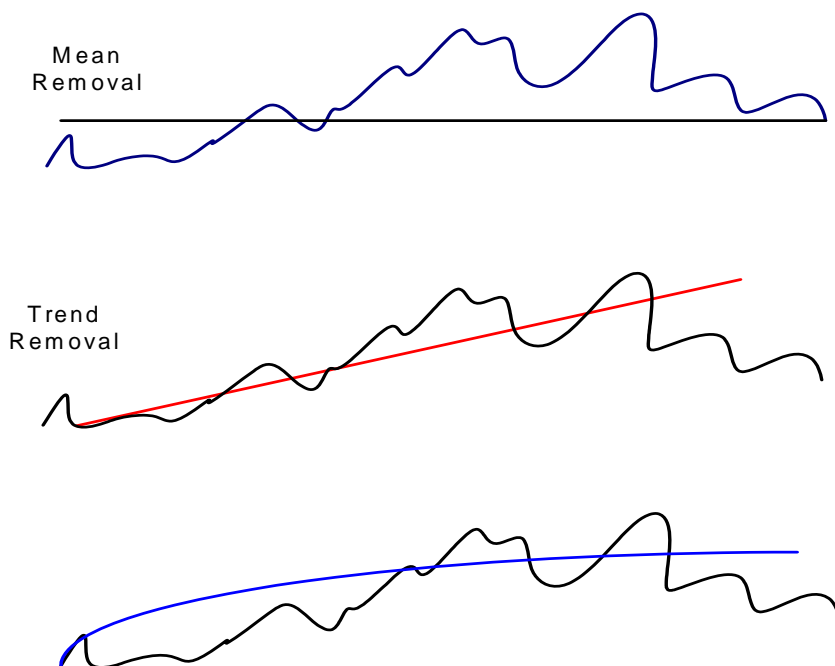

Figure 2 Representations of mean removal of turbulence time series

One can visualize the effects of removing means from time series by using transforms, such as the Fourier Transform, to convert time series from a temporal to frequency basis. In this transformed basis, we can examine the frequency at which fluctuations are passed or filtered.

ESPM 228, Advanced Topics in Biometeorology and Micrometeorology

Filters of interest include low-pass, high-pass and band-pass filters. There is a simple but distinct difference between the high and low pass filters. A low pass filter allows low frequencies to pass, but stops high frequencies. The simplest low pass filter is defined as:

$H(f)_{low} = 1, f < fc$
$H(f)_{low} = 0, f > fc$

A high pass filter is the opposite of the low pass filter, $H(f)_{high} = 1 - H(f)_{low}$.

An example of a high and low pass filter function is given in Figure 2. Note the low pass filter passes all signals with a frequency **lower** than a critical frequency, f_{crit}; in contrast the high pass filter passes frequencies **higher** than the critical value.

An additional point of information is that most band pass filters do not have such a perfect cut off (see Hamming, Digital Filters). This reality itself leads to numerical errors in the application of such filters. This point is discussed next.
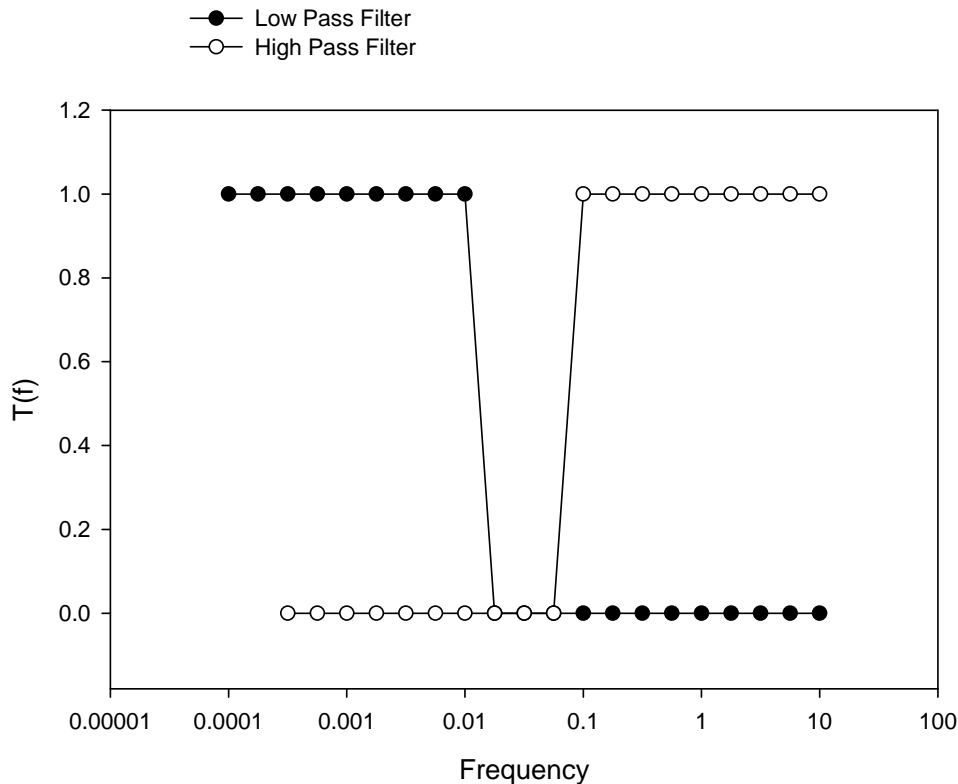

Figure 3 Example of low and high pass filter functions

The act of block-averaging a time series and using it to construct a series of fluctuation is equivalent to applying a square wave transfer function in temporal space.

$$h(t) = 1,$$

$$-\frac{T}{2} > t < \frac{T}{2}$$

$$h(t) = 0,$$

$$-\frac{T}{2} < t > \frac{T}{2}$$

where T is the averaging period, which typically ranges between 30 and 60 minutes. The Fourier transform of a square wave signal produces a transfer function that is a function of the sine function of the angular frequency. So a presumably 'clean' square wave averaging introduces sinusoidal noise at high frequencies. The Fourier transform of the Reynolds decomposition relations with an arithmetic mean yields a low pass transfer function:

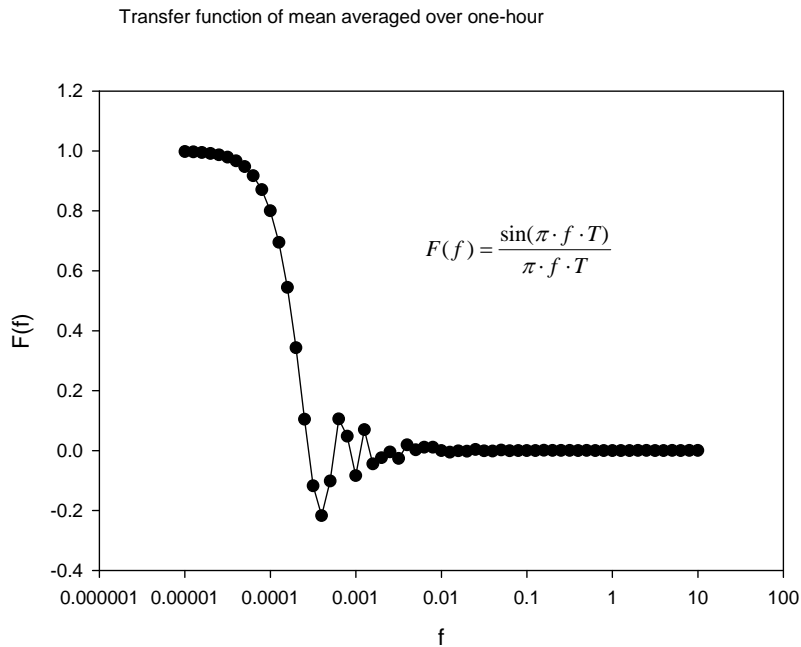$$F(f) = \frac{\sin(\pi \cdot f \cdot T)}{\pi \cdot f \cdot T}$$

Transfer function of mean averaged over one-hour

Figure 4 Transfer function for one hour average

When the filter function is applied to correct a power spectrum or co-spectrum the filter function is squared: $H(f) = F(f)^2$. If we want to compute fluctuations from the mean then we are subtract a mean value from the instantaneous values. This action imposes a high

ESPM 228, Advanced Topics in Biometeorology and Micrometeorology

pass filter upon the data. The resulting high pass transfer function is [*Kaimal and Finnigan*, 1994]:

$$H_{high\_pass}(f) = (1 - H(f))^2$$

$$\overline{w'c'}_{measured} = \int_0^\infty [1 - \frac{\sin^2(\pi \cdot f \cdot T)}{(\pi \cdot f \cdot T)^2}] H(\varpi) Co_{wc}(\varpi) d\omega$$

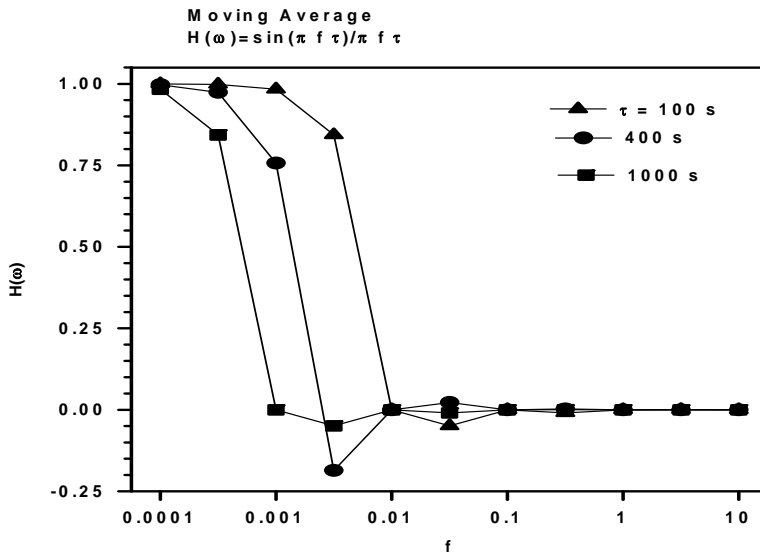Applying moving averages of shorter duration produces the following transfer functions.

Figure 5 Transfer function for block averaging. In this case the transfer function for a low pass filter is shown. Plotting 1-H(w) would provide information for the high pass filter.

Alternative Approaches to Computing Means

At the advent of eddy flux measurements, storage capacity of computers were quite small, or scientists had to use analog computers. One clever means of avoiding the storage of raw data, and later processing of means and covariances, was to compute means real-time with a digital recursive filter [*Dyer and Hicks*, 1972; *Massman*, 2000; *McMillen*, 1988].

Turbulent fluctuations are decomposed from the mean using as the difference between instantaneous (x_i) and mean ($\overline{x_i}$) quantities. An arithmetic mean or a running mean can be used to compute fluctuations. Computing the arithmetic mean, however, requires post

processing of the data. Mean values were determined in real-time, using a digital recursive filter:

$$\overline{x_i} = \alpha \overline{x_{i-1}} + (1-\alpha)x_i \qquad (1$$

where $\alpha = \exp(\dfrac{-\Delta t}{\tau})$, Δt is the sampling time increment and τ is the filter time constant.

Values of alpha for a range of time constants, assuming a 1/10 th second sampling interval (10 Hz) is listed below.

50	0.998002
100	0.999
200	0.9995
400	0.99975
800	0.999875
1600	0.999938

Theoretically, an optimal time constant can be chosen with the aid of a Fourier transform of the digital recursive filter. Massman [*Massman*, 2000] derived a spectrally dependent version of the transfer function as

$$\left| H(\omega) \right| = \frac{[\alpha + \alpha^2][1 - \cos(\omega / f_s)]}{(1 - 2 \cdot \alpha \cdot \cos(\omega / f_s) + \alpha^2)}$$
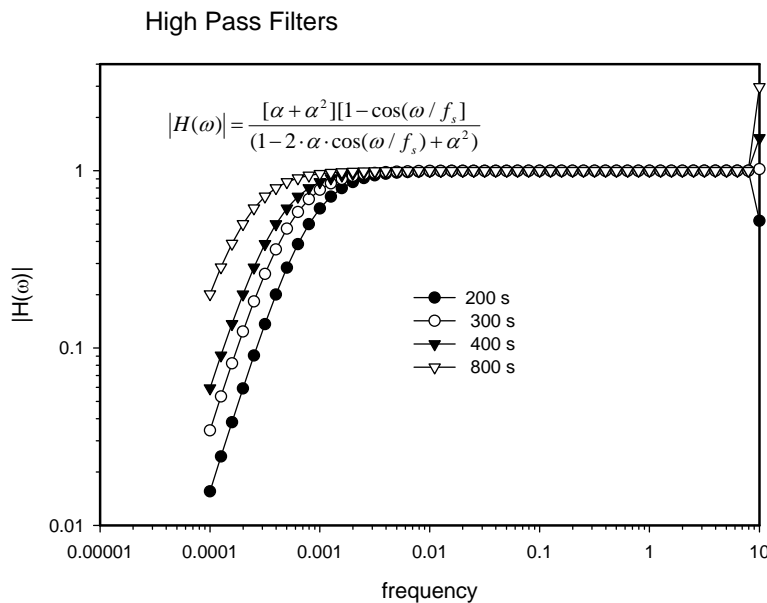

Figure 6 High pass transfer function of a digital recursive filter with various time constant The algorithm is from Massman [Massman, 2000].

8

Spectral cut off is not perfectly clean at low frequencies, but it lets some energy pass.

There remains uncertainty as to what the preferred value of the digital filter time constant should be inside a plant canopy.   We can examine this question by comparing eddy covariances computed with the various digital times constant against those computed with conventional Reynolds' decomposition and averaged over one-hour. We observe little differences (within 5%) between the two methods of compute flux covariances. Extending this analysis one step further, we observed that mass and energy flux covariance computations exhibit some sensitivity to the choice of filter time constant. Flux covariance computed with a 600s digital time constant is most ideal, while time constants between 400 and 800 s yielded covariance values that agreed within 5% of the Reynolds' flux covariance [*McMillen*, 1988].   Greatest numerical errors are associated with filter time constants less than 100s and more than 1000 s. This analysis was based on regressing the independent and dependent variables against one another, rather than plotting the ratios, which are numerically unstable when fluxes are small.
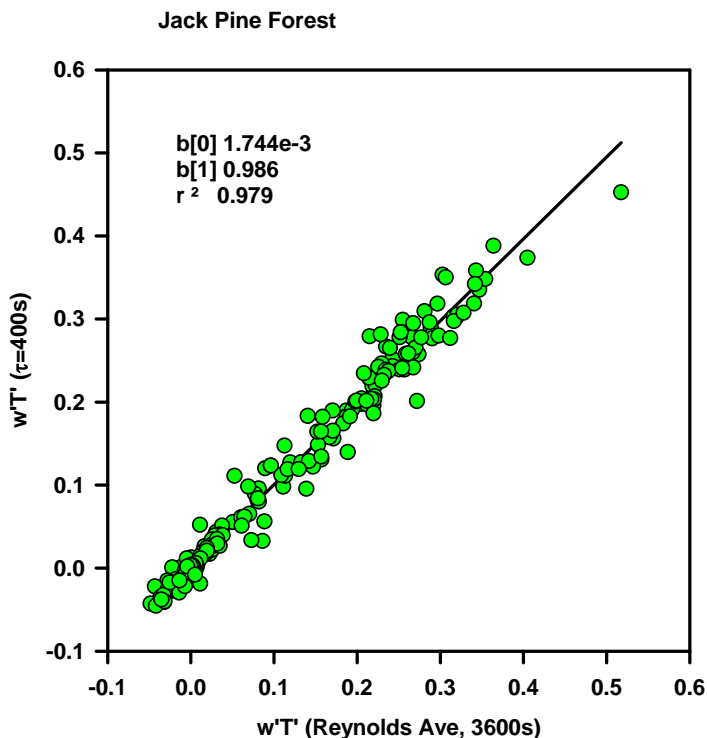
Jack Pine Forest

Figure 7 One to one plot of sensible heat flux covariance computed with conventional Reynolds averaging and with a digital recursive filter with a 400 s time constant.
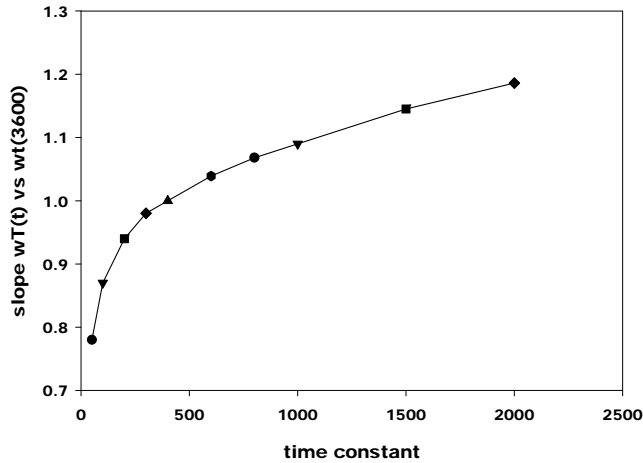
Figure 8 Slope of the relation of fluxes computed with a digital recursive filter and varying time constant and a 3600 s long time series, to which conventional Reynolds averaging was applied

In summary, a 400 to 600 s digital time constant is adequate to mimic the behavior of averaging over one hour. Interestingly, the critical time constant is close to $T/2\pi$, or 572 s.

One is not to confuse the concept of digital time constant with the averaging interval. Yet, there are many cases cited in the literature where one has used a 1000 s plus time constant. We have observed that exceeding long digital time constants can be problematic and error prone, too. This is a major reason why we have examined the Fourier transform of the filter to dispel this delusion.

Evaluating Short Term Fluctuations Digital Sampling at Limited Frequency

Computerized data acquisition systems digitize analog signals at discrete intervals. Discrete sampling of a time series, one which may consist of higher frequency contributions, limits the spectrum that can be resolved. The highest frequency is noted as the Nyquist frequency. It is defined as: $f_{Nyquist} = f_{sampling}/2$.

Ideally, we want to know the bandwidth of the turbulence spectra *a priori* and design the sampling strategy so we are able to sample at a frequency that is twice that of the highest frequency that significantly contributes to flux or variance. The following figure shows a typical spectrum for variance and flux. Over a tall forest the cut-off frequency may be as low as a few cycles per second.
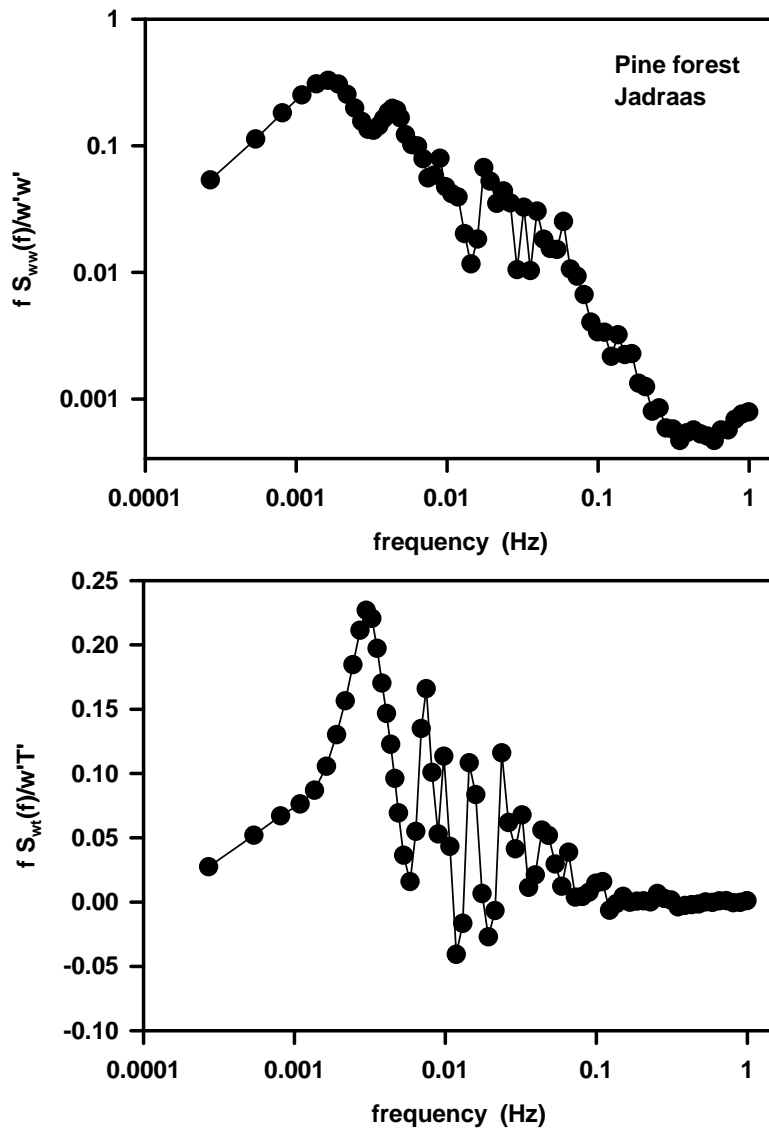
Figure 9 Vertical velocity power spectrum and w-T cospectrum over a Scots pine forest in Sweden.

The non-dimensional cutoff frequency is a function of measurement height, wind speed, stability and the natural spectral cutoff frequency: $f_c = n_c (z-d)/u$.   One can note from the figures above that the critical frequency of the co-spectrum occurs at a lower frequency than for the variance. This is because turbulence is isotropic in the inertial subrange of the power spectrum. If eddies have equal length and velocity scales in all direction, no material can be transferred at that scale. It is like a leaf in a whirl pool. It goes no where except round and round.

The minimum sampling rate can be adjusted by placing the sensors at a higher level if there are sensor time response constraints. Under neutral conditions the non-dimensional spectral cut-off for a power spectrum is on the order of about 5 to 10 Hz. What are typical values of the natural cutoff frequency, the one we must sample at in the field?

U	z	n
1	1	5
2	1	10
3	1	15
5	1	25
10	1	50
1	2	2.5
2	2	5
3	2	7.5
5	2	12.5
10	2	25
1	5	1
2	5	2
3	5	3
5	5	5
10	5	10
1	10	0.5
2	10	1
3	10	1.5
5	10	2.5
10	10	5

With regard to the cospectrum and flux measurements, isotropy associated with the inertial subrange (no material is transferred because motions in the x, y and z planes are equivalent), pushes significant eddies towards lower frequencies. Sampling restrictions are not as severe.

Sampling too slow leads to aliasing problems. Aliasing occurs when a high frequency signal appears as a lower frequency signal, since the harmonics of the high frequency signal are folded back on the lower frequency signals in the band between fs/2 and 0. This effect will distort the shape of the measured spectrum.

A common example of aliasing is the appearance of wagon wheels rotating backward on Western movies. Aliasing results in spurious energy or power being attributed to lower frequency eddies. In order to minimize aliasing the sampling rate should be at least 2 times the highest frequency of interest. This rule of thumb is derived from Shannon's sampling theorem says that at least 2 samples per cycle are needed to define the frequency component of that cycle.

ESPM 228, Advanced Topics in Biometeorology and Micrometeorology

We attempt to measure the whole spectrum of turbulence when designing and conducting an experiment. However, field measurements can suffer from the aliasing effects of 60 Hz AC noise if this information is significant and if it is not pre-filtered by analog means before digitization.
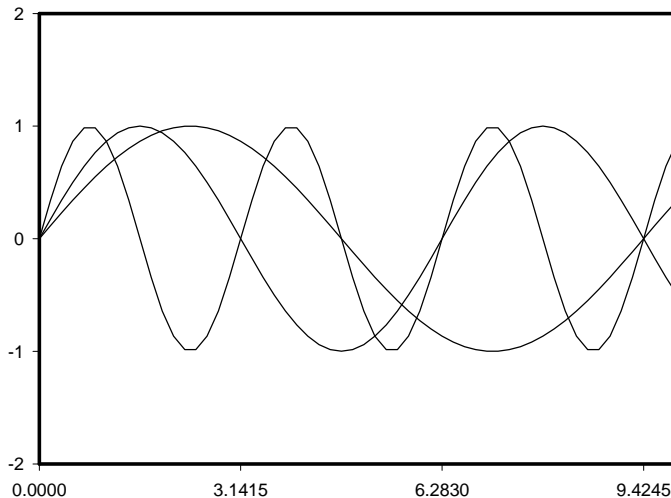

Figure 10 Visualization of aliasing, where high frequency components match and add to low frequency components. Shows the importance of high pass filtering before digitization of eddy flux data.

Analog pre-filtering using Butterworth, RC or Chebychev filters is helpful for removing environmental and electrical (AC 50 or 60 Hz) noise. This filtering was commonly done in early systems. Modern systems tend to already be filtered, so banks of analog filter systems tend not to be components of many systems today. But this is a feature to consider when designing and fabricating a system.

A filter function can be applied to compensate for the impact of aliasing [*Moore*, 1986].

$$H_{digitization}(f) = 1 + (\frac{f}{f_s - f})^3$$

This relation is valid for frequencies less than one-half the sampling frequency, $f <= f_s/2$

Electronic low pass filtering is performed to minimize aliasing. In action, it minimizes the folding of 'energy' from frequencies higher than the Nyquist frequency onto lower frequencies. This filter is not to be confused with the digital recursive filter we will use to remove running means. That one is applied at another end of the spectrum:

13

$$H_{lowpass}(f) = [1 + (\frac{f}{f_0})^4]^{-1}$$

Massman (2000), among others, argues that it is wrong to filter and correct for aliasing, as it is an artifact of digitization. Aliasing distorts the spectrum, but does not contribute to power or covariance; my mentor, Shashi Verma, also firmly stated that aliasing cannot be removed once an analog signal has been digitized.
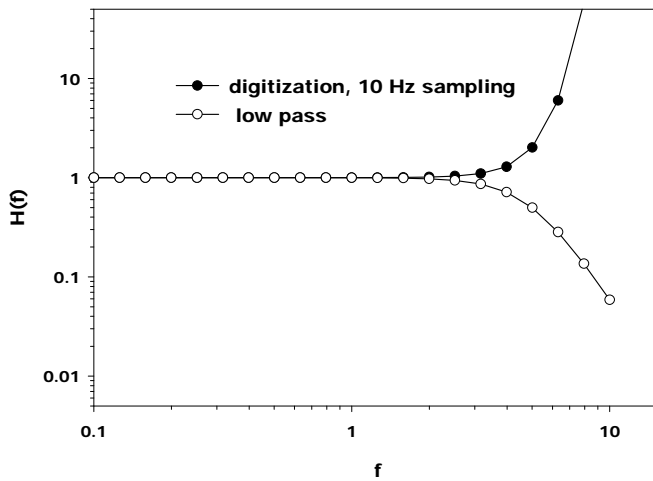

Figure 11 Low pass transfer function and spectrum

Sensor response

Mechanical instruments, like a cup anemometer, can impose a filtering effect on the process it measures. A cup anemometer will have a stall speed, below which it will not respond. If there is a dynamic pulse, there is a distance or time constant to which the instrument will react. A typical filtering function for a first order response is:

$$H_{sensor\_response}(f) = (1 + (2\pi f)^2 \tau_c^2)^{-1/2}$$

Key factors are the frequency and sensor time constant.

Tube dampening

ESPM 228, Advanced Topics in Biometeorology and Micrometeorology

Often, biometeorologists use a closed path sensor with a small tube that extends to near the volume of the sonic anemometer. Classic examples pertain to the measurement of CO2, methane, ozone, SO2 and water vapor. Ideas on sampling through a tube originated with theoretical studies by Taylor (1920s), Philip (1963). More modern treatments have been produced by Massman [*Massman*, 1991], Raupach and Lenschow [*Lenschow and Raupach*, 1991]and Leuning and Moncrieff[*Leuning and Moncrieff*, 1990].

The transfer function associated with samping through a tube is dependent on the tube radius (r), frequency (f) and diffusivity (D). If the dimensionless quantity, derived from these factors, is less than a critical value:

$$\frac{2\pi f r^2}{D_x} < 10$$

$$H_{tube\_dampening}(f) = \sqrt{\exp(x/6D_x u}$$

else the transfer function is one H(f)=1 *(see Leuning and King 1992).*

Massman reports a slightly different transfer function for turbulence flow:

$$H_{tube\_dampening}(f) = \exp(-4\pi^2 f^2 \Lambda L r u^{-2})$$

L is tube length,

For Re > 2300

$$\Lambda = 0.5\nu \text{Re} |\lambda_i| \Omega^{-1} D^{-1}$$

This case is valid for **laminar** flow, there is no dispersion of density fluctuations and they flow together with a velocity, denoted u. The problem with using laminar flow is that tube lengths and residence time in the tube needs to be short. Otherwise 'packets' of fluid start to diffuse and lose their coherence.

For laminar flow Re < 2100, Massman uses:

$$\Lambda = 0.0104\nu \text{Re} D^{-1}$$

The tube attenuation cutoff frequency

$$f_c = (0.008779 u^2 (\Lambda L r)^{-1})^{1/2}$$

Another attribute of sampling with turbulent flow is that a significant pressure drop is needed. In this situation, air is less apt to condense on the walls of the tube (Mike Goulden, personal communications).

The tube dampening correction does not correct for potential absorption/desorption of moisture by hygroscopic dirt particles in the tube or the diffusional loss of CO2 or water vapor through a tube.

The impact of sampling air with a closed or open path sensor has been quantified by several investigators [*Leuning and King*, 1992; *Leuning and Judd*, 1996; *Suyker and Verma*, 1993]. Sukyer and Verma have conducted extensive tests of open vs closed path sensors. There seems to be extensive line loss of water vapor. The problem is a function of tubing type and how dirty a tube is. Hygroscopic particles on a tube may be a reason. Today, no one has performed theoretical calculations about loss of water vapor as it flows down a tube due to permeability of the tube or absorption/desorption of hygroscopic particles. Leave this as a challenge for a precocious student.
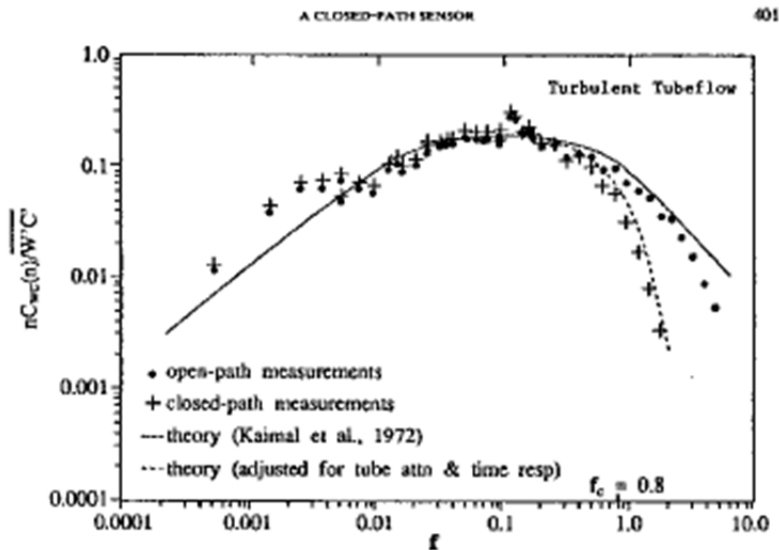

Fig. 3. Normalized logarithmic cospectra ($nC_{wc}(n)/\overline{w'\rho_c'}$) of CO_2 flux as a function of dimensionless frequency ($f = nz/U$). Included are cospectra measured with the open- and closed-path sensors, theoretical cospectrum for a scalar (Kaimal et al., 1972), the adjusted theoretical cospectrum (see Section 4.2.1 for details), and the cutoff frequency (f_c) for turbulent tubeflow (configuration II). August 17, 1990: 12:30–13:00 hr (local time). $z = 1.7$ m and $U = 3.9$ m s^{-1}.

Figure 12 Suyker and Verma. Spectral characteristics of eddy covariance computed with an open and closed path infrared gas analyzer.

ESPM 228, Advanced Topics in Biometeorology and Micrometeorology

In 1992, we conducted a study and compared open and closed IRGAs. In this case the agreement was reasonable, but the tube was short and the study was conducted only over 3 weeks, so the tube was relatively clean. Leuning et al reports that corrections for the effect of T fluctuations are not needed when one samples through a tube if temperature fluctuations are attenuated.
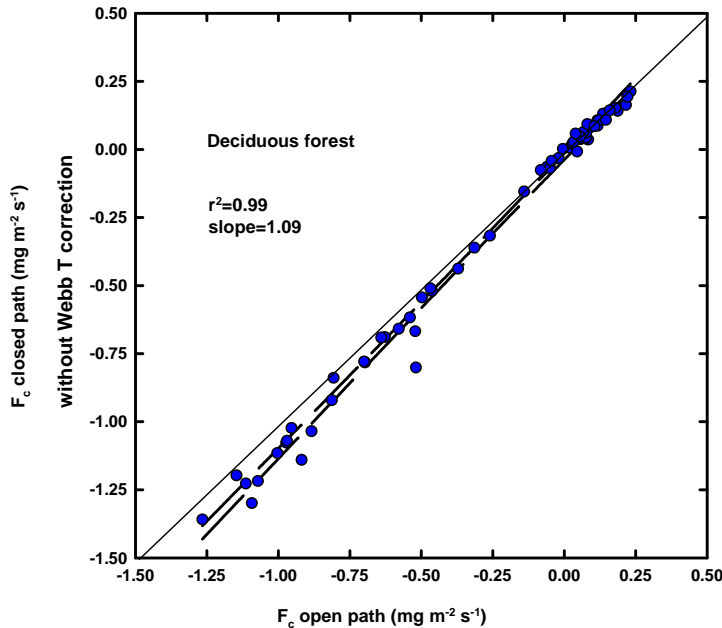

Figure 13 Comparision of an open and closed path IRGA to measure CO2 flux densities. (Baldocchi and Guenther, unpublished).

More recent and extensive measurements comparing open and closed path IRGAs by our group shows clear attenuation of $<w'q'>$ and $<w'c'>$ at a windy site and over an actively photosynthesizing and evaporating rice paddy. Here in this wet environment we see 20% reduction in water fluxes measured with closed path sensors, due to line attenuation. This hygroscopic filtering is hard to fix. My colleagues in France, so gradual degradation after a few days of using a new tube. The new LI7200 places the sensor on the tower and so it uses a very short tube. This may be a good solution to this otherwise nagging problem.

Twitchell Island

Twitchell Island
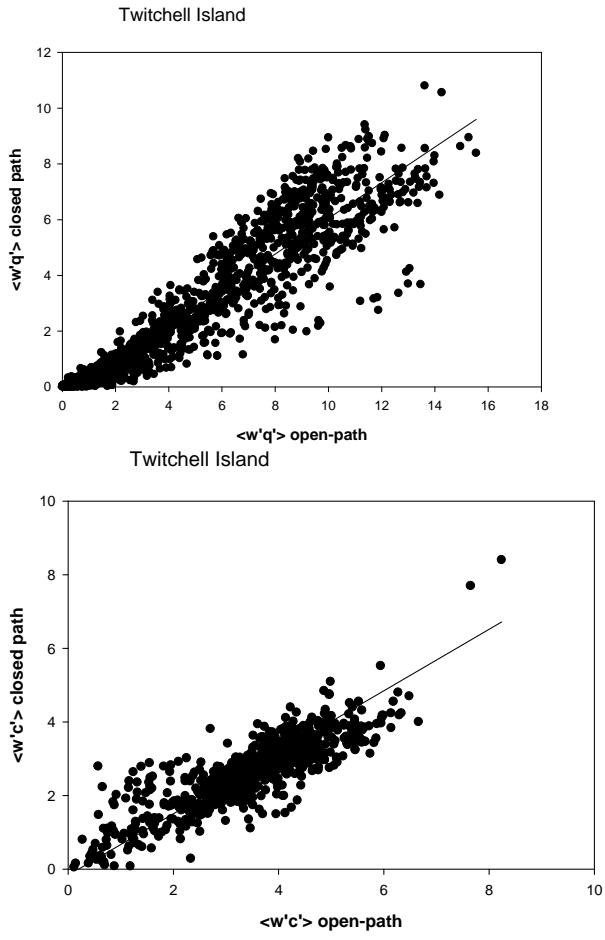
Comparison of the attenuation of sampling methane co-spectrum through a closed and open sensors is seen below.
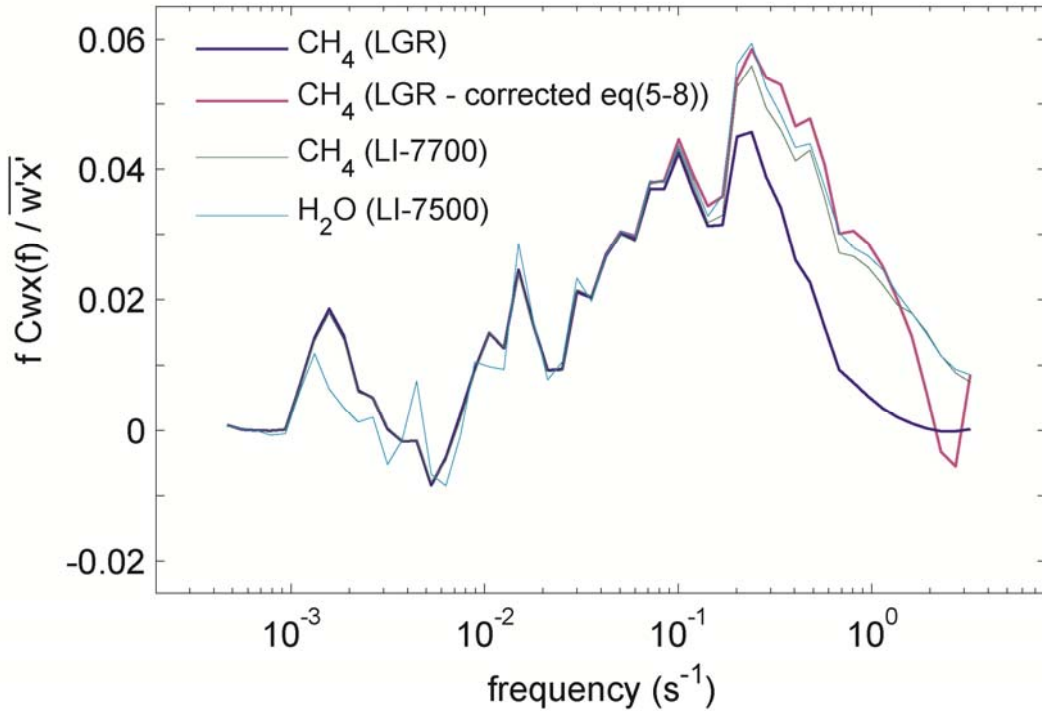
On annual time scales, Haslwanter et al report [*Haslwanter et al.*, 2009] that the closed path system yielded more positive net ecosystem exchange (25 gC m-2 y-1) than an open path system (0 gC m-2 y-1), and lower evaporation totals (465 mm yr-1) compared with the open path system (549 mm y-1). In practice more data from open path systems will be excluded over a year due to rain, dew, fog etc. and the closed path system can be calibrated regularly.

Sensor Line Averaging

Sonic anemometers and infrared gas analyzers have finite sensor paths. These path lengths smear smaller eddies. One cannot detect frequencies smaller than the pathlength, which is why small hot wire anemometers are used to measure finer scale turbulence. One proposed transfer function for sensor line averaging was proposed by Van den Hurk (1995):

$$H_{pathave}(f) = \frac{1}{2\pi f}(3 + \exp(-2\pi f) - 4\frac{1 - \exp(-2\pi f)}{2\pi f})$$

here f is a normalized frequency, nd/u, where d is the path length.

ESPM 228, Advanced Topics in Biometeorology and Micrometeorology

Sensor Separation

The velocity and scalar sensors should be co-located to minimize a decorrelation as an eddy of a given size passes through the sensor array. Yet care must be made to minimize the scalar sensor from distorting the flow sensed by the anemometer.
Kristensen [*Kristensen et al.*, 1997] recommends that the separation distance d < (z-d)/5
Kaimal recommends a more conservative metric, d=(z-d)/6π. More recently, Lee and Black report that error is less than 3% if the ratio between separation distance and z-d is less than 5%.

If one is interested in computing the transfer function for sensor separation, one can simulate it with the following algorithm:

$$H(x)_{sensor\_separation} = \exp(-9.9x^{1.5})$$

x is a normalized frequency (fs/u)

There are new questions about where to place an open path irga relative to a sonic anemometer. Kristensen et al [*Kristensen et al.*, 1997] recommends placing it below the anemometer, but in the same vertical access. If it is displaced horizontally, there will be a time lag (d/u) based on the wind speed and the spatial separation. They state that the loss of flux will be less than 1% if the displacement at 10 m is 0.2 m, but it can be 13% if the instrument is at 1 m. In the vertical, the loss is 18% if the scalar sensor is displaced above the sonic, but only 2% if the scalar sensor is 0.2 m below the sonic anemometer. They conclude that when sampling near the ground vertical separation is preferred with the scalar sensor below the anemometer. This keeps a symmetric configuration.

The Total Transfer Function

Moore reports net transfer functions as

$$T_{data\_acquisition} = H_{aliasing}H_{high\_pass}H_{low\_pass}$$

$$T_{measurement} = H_{sensor\_separation}H_{instrument\_response}\sqrt{H_{path\_ave\_chem\_sensor}H_{path\_ave\_w}H_{tube\_dampening}}$$

So the total transfer function for CO2 flux would be

$$T_{total}(\varpi) = T_{data\_acquisition}(\varpi)T_{measurement}(\varpi)$$

A basic version of the Moore code is provided on the course web page for use and implementation,
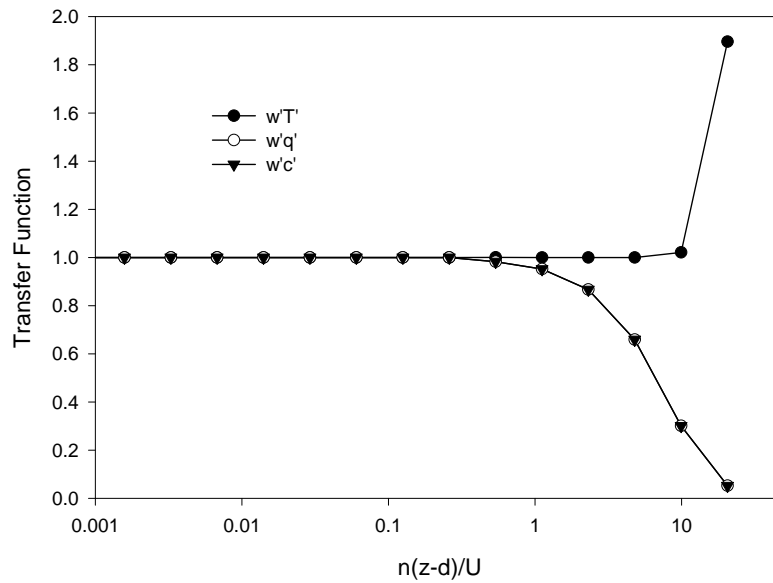
Figure 14 Examples of integrated transfer function for heat, water vapor and

Improper spectral response can be compensated two ways. One is to correct the flux covariance by the ratios of the observed spectrum and some 'perfect' measure, such as the acoustic temperature co-spectrum. This method is used by the group at Harvard Forest, for example. Two down sides with this approach. It does not account for line averaging, which occurs because of the fit distance of the anemometer path, and fails with sensible heat flux density is near zero.

The other approach involves quantifying the appropriate transfer functions and using them to correct the eddy covariance method. This approach was developed by Moore in 1986 and has recently been modified by Massman [*Massman*, 2000]. It is based on certain assumptions about the co-spectral shape of turbulent transfer. Most recently, Massman (2000) derived an analytical version of the numerical transfer functions originally posited by Moore (1986). The general equation is:

$$\frac{\overline{w'c'}_m}{\overline{w'c'}} = \left[\frac{ab}{(a+1)(b+1)}\right]\left[\frac{ab}{(a+p)(b+p)}\right]\left[\frac{1}{(p+1)}\right]\left[1-\frac{p}{(a+1)(a+p)}\right]$$

where $a = 2\pi f_x \tau_h$ and is a function of the time constant for the trend removal

$b = 2\pi f_x \tau_b$ and is a function of the time constant for the block average removal

$p = 2\pi f_x \tau_e$ and is a function of the first order time constant

$$f_x = \frac{n_x u}{z}$$

For z/L < 0 $n_x = 0.085$

Massman's relation does not account for aliasing or vertical displacement of sensors.

The transfer functions are then used estimate and correct the relative error in an eddy covariance measurement. With this approach one computes:

$$\frac{\Delta F_c}{F_c} = 1 - \frac{\int\limits_{0}^{\infty} H_{wc}(\omega) S_{wc}(\omega) d\omega}{\int\limits_{0}^{\infty} S_{wc}(\omega) d\omega}$$

For engineering purposes, Kaimal et al. derived equations for predicting spectral shapes under near neutral conditions

$$\frac{n S_w(n)}{u_*^2} = \frac{2.1n}{1 + 5.3 n^{5/3}}$$

$$\frac{n S_u(n)}{u_*^2} = \frac{102n}{(1 + 33n)^{5/3}}$$

$$\frac{n S_v(n)}{u_*^2} = \frac{17n}{(1 + 9.5n)^{5/3}}$$

The spectrum of turbulence also scales with stability. The spectral peak shifts toward larger wavelengths with convective conditions. Thermals scale with the depth of the pbl, hence the shift towards longer wavelengths.
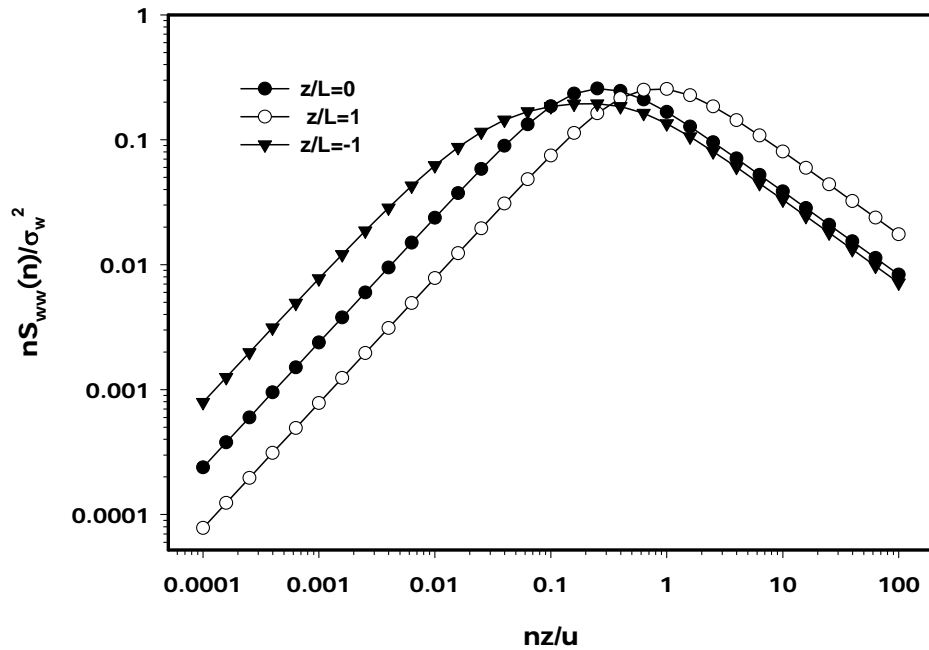
Figure 15 Computations of Spectra as a function of stability, using the Kaimal

functions

Numerous functions exist in the literature for co-spectra, too, starting with the famous Kansas experiment.

$$nS_{wx}(n) = \frac{f}{A + Bf^{2.1}}$$

The coefficients A and B very with stability. We also assume co-spectral similarity, in that the spectra for heat, water and CO_2 are identical.

Accumulating data taken over tall forests also show evidence of a spectral shift, as compared to idea conditions simulated by the Kaimal spectra.

A few new comments should be raised about the classical Kaimal spectra. First they were developed over very flat, ideal landscape. Secondly they were developed on the basis of about 45 hours of data. More recently, Kai Morgenstern has used data from the Fluxnet project to examine turbulence spectra over 100,000s+ hours of data and from about 20 field sites. Detto et al. [*Detto et al.*, 2010] provide the newest set of algorithms for

spectra under stable, near neutral and unstable thermal stratification from thousands of hours of measurements and for u, T, q, CO2 and CH4.

I terms of wavenumber the spectral equation is

$$S(\kappa) = S_0(\kappa)(1 + \kappa \cdot \kappa_m)^\gamma$$

For shorthand we provide the matices of coefficients for `u, T, H2O, CO2, CH4,` `indexed j=1,2,3,4,5, and for stable, near neutral, unstable` `thermal stratification, indexed i = 1,2,3....`

```
% S0 power spectra
S0(1, :) = [4,2.5,3.1,1.6,0.4];   % stable
S0(2,:) = [8,5.3,3.8,2.9,0.2];    % near neutral
S0(3,:) =[8.9,6.8,5.2,3.9,2.3];   % unstable


% km power spectra (m^-1)
km(1,:)= [4,3.1,4.3,3.1,2.1];     % stable
km(2,:)=[11.1,12.3,9.3,10.5,1.4]; % near neutral
km(3,:)=[14.2,16.8,12.2,14.8,15.2]; % unstable


% gamma, v, power spectra

v(1,:)=[1.7,1.5,1.6,1.3,1]; % stable
v(2,:)=[1.6,1.2,1.4,1.2,1]; % near neutral
v(3,:)=[1.6,1.3,1.4,1.2,1.3]; % unstable


% S0 c spectra
Co.S0(1,:) = [4,2.5,3.1,1.6,0.4]; % stable
Co.S0(2,:) = [8,5.3,3.8,2.9,0.2]; % near neutral
Co.S0(3,:) =[8.9,6.8,5.2,3.9,2.3]; % unstable

% km power co spectra
Co.km(1,:)= [4,3.1,4.3,3.1,2.1]; % stable
Co.km(2,:)=[11.1,12.3,9.3,10.5,1.4]; % near neutral
Co.km(3,:)=[14.2,16.8,12.2,14.8,15.2]; % unstable

% gamma, v, co spectra

Co.v(1,:)=[1.7,1.5,1.6,1.3,1];
Co.v(2,:)=[1.6,1.2,1.4,1.2,1];
Co.v(3,:)=[1.6,1.3,1.4,1.2,1.3];
```
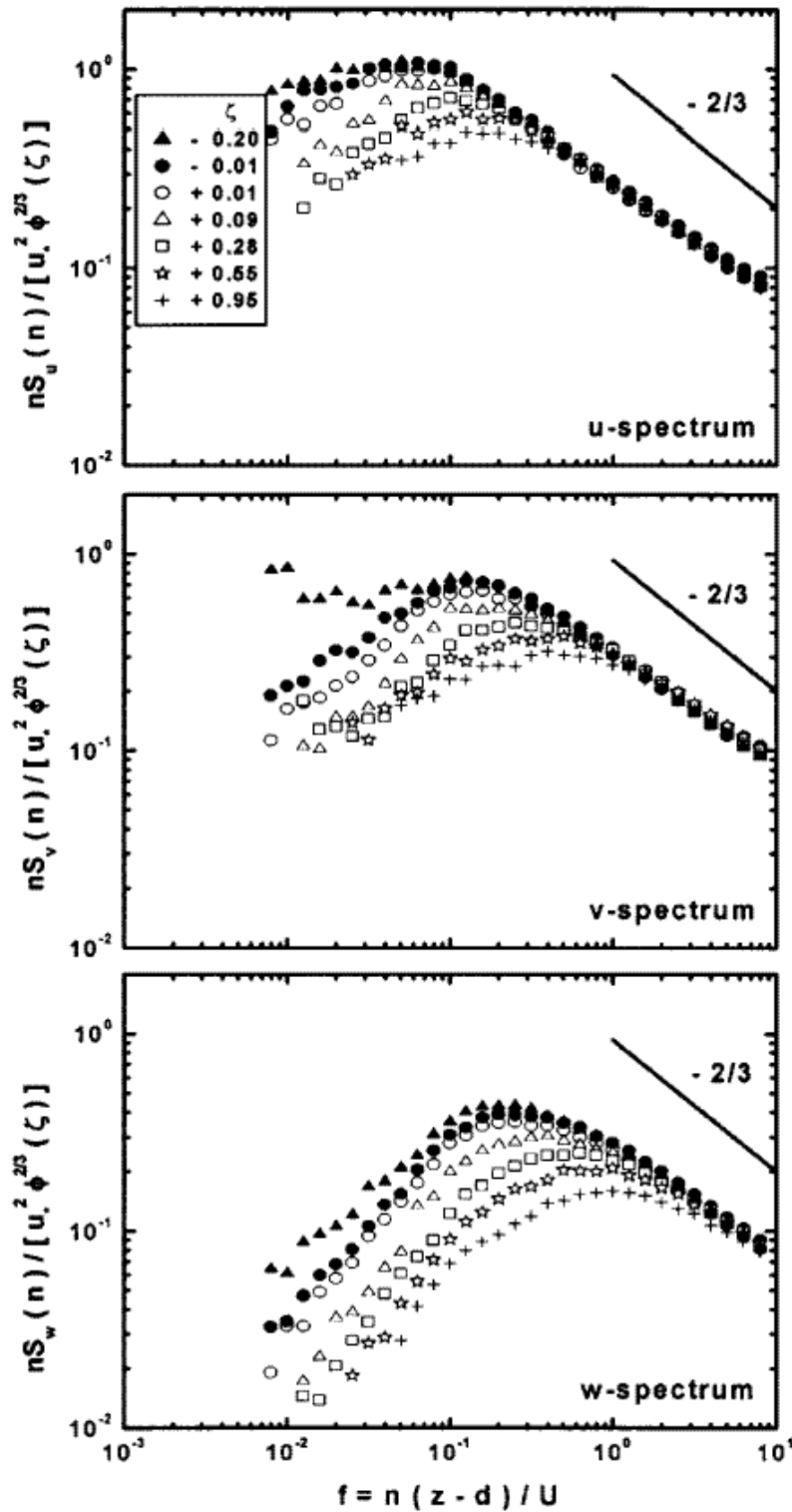
igure 4. Normalized velocity spectra. Data shown are for the foliated period at the 46-m level of the MBS site.

Figure 16 Su et al 2004 BLM

Appendix

The Fourier transform $(S_{xx}(\omega))$ at a particular angular frequency $(\omega = 2\pi f$, radians per second; f is natural frequency; cycles per second) of a stochastic time series $(x(t))$ is defined as:

$$S_{xx}(\varpi) = \int_{-\infty}^{\infty} x(t) \exp(i\varpi t) dt \quad (1$$

In Equation 1, i is the imaginary number, $\sqrt{-i}$. One attribute of examining Fourier transforms is that, according to Parseval's theorem, the variance (σ_x^2) is related to the integral of the power spectrum with respect to angular frequency:

$$\sigma_x^2 = \int_{-\infty}^{\infty} |S_{xx}(\varpi)|^2 \, d\varpi \quad (2$$

It thereby allows us to examine the amount of variance associated with specific frequencies.

Remember

$$\exp(ix) = \cos x + i \sin x$$

$$\exp(-ix) = \cos x - i \sin x$$

$$|\exp ix| = 1$$

$$\cos x = \frac{1}{2} [\exp(ix) + \exp(-ix)]$$

$$\sin x = \frac{1}{2} [\exp(ix) - \exp(-ix)]$$

So the Fourier expansion series:

$$f(\varpi) = \frac{A_0}{2} + \sum_{k=1}^{N} A_k \cos k\varpi + \sum_{k=1}^{N} B_k \sin k\varpi +$$

The spectral relation between two independent, but simultaneous, time series was quantified with a co-spectral analysis. The co-spectra derived from the cross spectrum $(S_{xy}(\omega))$ between two time series, $x(t)$ and $y(t)$. The cross spectrum is a function of the cross-correlation function, R_{xy}:

$$S_{xy}(\varpi) = \frac{1}{\pi} \int_{-\infty}^{\infty} R_{xy}(\tau) \exp(i\varpi\tau) d\tau \quad (3$$

The cross-correlation between $x(t)$ and $y(t+\tau)$ is computed as:

$$R_{xy} = (T \xrightarrow{\text{lim}} \infty) \frac{1}{2T} \int_{-T}^{T} x(t)y(t+\tau) dt \quad (4$$

The cross-spectrum has an even and odd component:

$$S_{xy}(\varpi) = Co_{xy}(\varpi) + iQ_{xy}(\varpi) \quad (5$$

The even component of the cross spectrum yields the co-spectrum, $Co_{xy}(\omega)$):

$$Co_{xy}(\varpi) = \frac{1}{\pi} \int_{-\infty}^{\infty} R_{xy}(\tau) \cos(\varpi\tau) d\tau \quad (6$$

and the odd component yields the quadrature, $Q_{xy}(\omega)$), spectrum:

$$Q_{xy}(\varpi) = \frac{1}{\pi} \int_{-\infty}^{\infty} R_{xy}(\tau) \sin(\varpi\tau) d\tau$$

Fundamentally, these calculations are performed on discrete and evenly-spaced, time series. The specific frequencies that can be decomposed from such a time series are defined from $f_n = n / (N\Delta t)$, where the time step between samples is Δt, the total number of samples is denoted as N and the index n varies from –N/2 to +N/2. The discrete Fourier transform (F_x) for for a time series ($f(n)$) at a time index number k is:

ESPM 228, Advanced Topics in Biometeorology and Micrometeorology

$$F_x(k) = \sum_{n=0}^{N-1} f(n)\exp(-i2\pi nk/N) \quad (9$$

The power spectrum is a function of the Fourier transform and its complex conjugate $S_x(k) = \dfrac{\Delta t}{N} F_x(k) F_x^*(k)$. The co-spectrum and quadrature spectrum between two variables, x and y, are computed in a related manner, with respect to the real ($Co_{xy}(k) = \text{Re}(\dfrac{\Delta t}{N} F_x(k) F_y^*(k))$) and imaginary ($Q_{xy}(k) = \text{Im}(\dfrac{\Delta t}{N} F_x(k) F_y^*(k))$) components.

Bibliography

Denmead, O.T. 1983. Micrometeorological methods for measuring gaseous losses of nitrogen in the field. In: Gaseous Loss of Nitrogen from plant-soil systems. eds. J.R. Freney and J.R. Simpson. pp 137-155.

Lenschow, DH. 1995. Micrometeorological techniques for measuring biosphere-atmosphere trace gas exchange. In: Biogenic Trace Gases: Measuring Emissions from Soil and Water. Eds. P.A. Matson and R.C. Harriss. Blackwell Sci. Pub. Pp 126-163.

Wesely, M.L. 1970. *Eddy correlation measurements in the atmospheric surface layer over agricultural crops*. Dissertation. University of Wisconsin. Madison, WI.

Wesely, M.L., D.H. Lenschow and O.T. 1989. Flux measurement techniques. In: Global Tropospheric Chemistry, Chemical Fluxes in the Global Atmosphere. NCAR Report. Eds. DH Lenschow and BB Hicks. Pp 31-46.

Endnote References

Aubinet, M., et al. (2000), Estimates of the annual net carbon and water exchange of Europeran forests: the EUROFLUX methodology, *Advances in Ecological Research*, *30*, 113-175.
Baldocchi, D. D. (2003), Assessing the eddy covariance technique for evaluating carbon dioxide exchange rates of ecosystems:past, present and future., *Global Change Biol*, *9*, 479-492.
Baldocchi, D. D., B. B. Hicks, and T. P. Meyers (1988), Measuring biosphere-atmosphere exchanges of biologically related gases with micrometeorological methods, *Ecology.*, *69*, 1331-1340.
Businger, J. A. (1986), Evaluation of the Accuracy with Which Dry Deposition Can Be Measured with Current Micrometeorological Techniques, *Journal of Climate and Applied Meteorology*, *25*(8), 1100-1124.

Detto, M., D. Baldocchi, and G. G. Katul (2010), Scaling Properties of Biologically Active Scalar Concentration Fluctuations in the Atmospheric Surface Layer over a Managed Peatland, *Boundary-Layer Meteorology*, *136*(3), 407-430.

Dyer, A. J., and B. B. Hicks (1972), Spatial Variability of Eddy Fluxes in Constant Flux Layer, *Q. J. R. Meteorol. Soc.*, *98*(415), 206-&.

Foken, T., and B. Wichura (1996), Tools for quality assessment of surface-based flux measurements, *Agricultural and Forest Meteorology*, *78*(1-2), 83-105.

Goulden, M. L., J. W. Munger, S. M. Fan, B. C. Daube, and S. C. Wofsy (1996), Measurements of carbon sequestration by long-term eddy covariance: Methods and a critical evaluation of accuracy, *Global Change Biology*, *2*(3), 169-182.

Haslwanter, A., A. Hammerle, and G. Wohlfahrt (2009), Open-path vs. closed-path eddy covariance measurements of the net ecosystem carbon dioxide and water vapour exchange: A long-term perspective, *Agricultural and Forest Meteorology*, *149*(2), 291-302.

Horst, T. W. (1997), A simple formula for attenuation of eddy fluxes measured with first-order-response scalar sensors, *Boundary-Layer Meteorology*, *82*(2), 219-233.

Kaimal, J. C., and J. J. Finnigan (1994), *Atmospheric Boundary Layer Flows*, 302 pp., Oxford University Press.

Kristensen, L., J. Mann, S. P. Oncley, and J. C. Wyngaard (1997), How close is close enough when measuring scalar fluxes with displaced sensors?, *Journal of Atmospheric and Oceanic Technology*, *14*(4), 814-821.

Lenschow, D. H., and M. R. Raupach (1991), The Attenuation of Fluctuations in Scalar Concentrations through Sampling Tubes, *J. Geophys. Res.-Atmos.*, *96*(D8), 15259-15268.

Leuning, R., and J. Moncrieff (1990), Eddy-Covariance Co2 Flux Measurements Using Open-Path and Closed-Path Co2 Analyzers - Corrections for Analyzer Water-Vapor Sensitivity and Damping of Fluctuations in Air Sampling Tubes, *Boundary-Layer Meteorology*, *53*(1-2), 63-76.

Leuning, R., and K. M. King (1992), Comparison of Eddy-Covariance Measurements of Co2 Fluxes by Open-Path and Closed-Path Co2 Analyzers, *Boundary-Layer Meteorology*, *59*(3), 297-311.

Leuning, R., and M. J. Judd (1996), The relative merits of open- and closed-path analysers for measurement of eddy fluxes, *Global Change Biology*, *2*(3), 241-253.

Loescher, H. W., B. E. Law, L. Mahrt, D. Y. Hollinger, J. Campbell, and S. C. Wofsy (2006), Uncertainties in, and interpretation of, carbon flux estimates using the eddy covariance technique, *J. Geophys. Res.-Atmos.*, *111*(D21), doi:10.1029/2005JD006932.

Massman, W. J. (1991), The Attenuation of Concentration Fluctuations in Turbulent-Flow through a Tube, *J. Geophys. Res.-Atmos.*, *96*(D8), 15269-15273.

Massman, W. J. (2000), A simple method for estimating frequency response corrections for eddy covariance systems, *Agricultural and Forest Meteorology*, *104*(3), 185-198.

Massman, W. J., and X. Lee (2002), Eddy covariance flux corrections and uncertainties in long-term studies of carbon and energy exchanges, *Agricultural and Forest Meteorology*, *113*(1-4), 121-144.

McMillen, R. T. (1988), An Eddy-Correlation Technique with Extended Applicability to Non-Simple Terrain, *Boundary-Layer Meteorology*, *43*(3), 231-245.

Moore, C. J. (1986), Frequency response corrections for eddy covariance systems., *Boundary Layer Meteorology*, *37*, 17-35.

Suyker, A. E., and S. Verma (1993), Eddy correlation measurements of CO_2 flux using a closed path sensor-theory and field-tests against an open-path sensor, *Boundary-Layer Meteorology*, *64*, 391-407.